

## **A Rapid and Effective Screening of Chiral Drug Delivery within the Effect of Vascular Environment by Molecularly Imprinted Polymers**

**Roongnapa Suedee**

**Sirirat Rakkit**

Molecular Recognition Materials Research Unit  
NANOTEC-PSU Center of Excellence on Drug Delivery System  
Department of Pharmaceutical Chemistry  
Faculty of Pharmaceutical Sciences  
Prince of Songkla University  
Hat Yai, Songkhla 90112  
Thailand

**Alongkot Treetong**

National Nanotechnology Center (NANOTEC)  
National Science  
Technology Development Agency (NSTDA)  
Thailand Science Park  
Phahonyothin Road, PathumThani 12120  
Thailand

### **Abstract**

*In this study, we developed a molecularly imprinted polymer (MIP) that screened platforms to quantify the drug delivery through changes of environment into the blood component. The enhanced surface interactions between the tinplating species and thalidomide were identified by Atomic Force Microscopy as well as force analysis. Overall, the results demonstrate that the approach can affect efficient binding sites through which the MIPs can perform well, clearly indicated distinguishing the different compounds selectively traversed from the whole blood. Detailed examination revealed the surface rearrangements in the presence of the template during polymerization influenced efficient binding sites for (R)-form to penetrate into the protein complex on the RMIP, yet that appeared a substantially marked (S)-form, localized on the SMIP. Therefore the configure biomimesis-MIP approach can be successfully applied for facilitating drug infusion would hold promise for improving of drug delivery.*

**Keywords:** molecularly imprinted polymers; multi-step swelling; drug infusion; configuration biomimesis; nanoscience; enhanced surface probe

### **1. Introduction**

Molecular imprinting is a useful technique that enables the creation of biomimetic receptors for molecular recognition and may also allow for opportunities to investigate the substrate-binding events of pharmaceutically relevant compounds. The imprinting into a polymeric system can lead to a tailored-making or imitate, as it is one of the promising technique of a molecular memory (Krysio and Peppas, 2012; Karlsson et al., 2009). Biomimetic sensor is a viable alternative for a response to a specific molecule released under suitable environment, has drawn much attention in the field of nanoscience and nonmaterial over the past few years. The advantage of synthetic recognition material allowed switching the coordinated assemblies of the frameworks serves as a sensing system is highly to assess compounds in complexity of living system (Arabi, Ghaedi and Ostovan, 2017).

This is because of chemically identical compounds with different stereo configurations have different interactions with natural receptors, enzymes and other binding molecules (Liang, Wu and Deng, 2016). In addition, each of the stereoisomer's will have their own unique binding sites that imprinting technology is capable of fabricating mimics for the natural sites. The imperative advantage of molecular imprinting technology is that it is being pursued by processes that of introducing of complementary counterparts and selective sites that derived both from matching the shape and from having the appropriate arrangement after template removal. Strategy of designed system may even facilitate the development of the sensitive co-ordinate framework with excellent recognition ability (Xing et al., 2017). In addition, surface imprinting technique provides the strategy to incorporate molecular recognition ability, allows rapid recognition event is highly useful for differential biomacromolecule analysis (Chen, Rick and Chou, 2009; Eersels, Lieberzeit and Wagner, 2016). The application of molecular imprinting has been useful in many fields of research such as drug delivery (Byrne, Hilt and Peppas, 2008), diagnostics (Bellagha-Chenchah et al., 2015), drug analytical applications (Sellergren 1994; Owens et al., 1999), environmental science (Suedee, Intakong and Dickert, 2006) and for the development of a material for target analysis in blood (Tebane and Batlokwa, 2017).

Due to a new approach of sensitive screening of specific compounds by molecular imprinting, that uses anti-TNF- $\alpha$ , (*R*)- or (*S*)-thalidomide as the templates. Thalidomide and analogs are an immunomodulatory drug and it is an effective treatment against erythematous nodules, multiple myeloma, HIV-related diseases (Hattori and Iguchi, 2004). The use of thalidomide shows good results in the treatment of diseases. Nevertheless, the success in the assessment of the drug delivery in the presence of protein matrix is important due to toxicities; as (*S*)-thalidomide has teratogenic effects cause by target (*i.e.* ceramide) inhibiting in production of chicks and zebra fish (Beedie et al., 2016). In addition the assessment of target analyses relies on rapid and sensitive technique. This is because the disease stages or induced vascular environment for therapy, or even boost activity of known therapeutic can primarily stimulate some molecules selectively traverse through blood (Vyacheslav, Stephen and Bradford, 2007). It is well known that proteolipid caused the coronary disorder, which avoid the damage in tissues and the endothelial organs. The exposed blood disorder render the measurements are difficult for the analyte inclusion. The use of advanced techniques such as flow cytometry and stem cell-culture assays, are very expensive and time consuming. It is urgent need to develop an effective technique for removal of the contamination of interferences for the blood analysis. Within this work, we exploited configurational biomimesis imprinting approach, that all of the MIP materials would be screened. Thalidomide had an antagonistic activity via the sphingosine-1-phosphate pathway (*i.e.*, DNA, coordination polymers) (Yabu et al., 2005) which was relevant to the chemical functional groups used in the study. The design with such functionality, an expanded ability on the binding cavities could be achieved *via* structural features of the 'target' molecules. The energetic advantage of the approach is the variation of surface properties that may increase more efficient drug-MIP upon changes of vascular environment for drug delivery application. The goal of this work is to determination of corresponding changes of differential measurement in impedances when a single thalidomide enantiomer was exposed to MIPs on the sensor. The analysis of AFM images and force measurement were performed with and without the blood component. To be our best knowledge, MIP for an enhanced surface method which this technique would produce a rapid screening and determining for the target analyses into the vascular environment and to enable the detail information at the same time.

## 2. Experiment and methods

### 2.1. Chemicals and materials

Styrene, methacrylic acid (MAA), 1-vinyl-2-pyrrolidone (NVP), *N,N'*-(1,2-dihydroxyethylene) bisacrylamide (DHEBA), polycaprolactone triol (PCL-T), sodium lauryl sulfate (SLS), disodium ethylenediaminetetraacetic acid (EDTA), ethylene glycol dimethacrylate (EDMA), trimethylolpropanetri-methacrylate (TRIM), thioglycolate, human serum albumin, (*S*)-(-)-thalidomide, (*R*)-(+)-thalidomide, and racemic ( $\pm$ )-thalidomide were procured from Aldrich Chemical Company (Milwaukee, WI, USA). 2,2'-Azobisisobutyronitrile (AIBN) was obtained from Wako Pure Chemical Industries (Osaka, Japan). Cholesterol, bovine serum albumin, and ceramide were purchased from Aldrich Chemical Company (Milwaukee, WI, USA). Dibutyl phthalate, potassium peroxydisulfate, and polyvinyl alcohol (PVA) were obtained from Fluka Chemie (Buchs, Switzerland). MAA was purified by distillation under reduced pressure before use. All other solvents used were of analytical reagent grade and used without further processing.

## 2.2. Preparation of MIPs and NIPs

MIPs selective for (*R*)-thalidomide and (*S*)-thalidomide were prepared via a multi-step swelling polymerization as previously reported, with slight modifications (Haginaka et al., 1998). In a typical MIP preparation of the preformed (polystyrene) particles (1.0 g, approximately 0.96  $\mu\text{m}$  in diameter of polystyrene), which was obtained by thermal polymerization in the presence of peroxydisulfate as the initiator, was mixed with dibutyl phthalate (0.6 mL, 2 mmol), sodium lauryl sulfate (0.02 g, 0.07 mmol), and distilled water (6 mL). Subsequently, this suspension was stirred (125 rpm) at room temperature ( $25 \pm 1^\circ\text{C}$ ). After 20 h, the monomeric mixture was prepared from the components of the polymerization reaction (Table 1), and 6 mL of toluene was added to the mixture. Then, 12.0 mL of distilled water was admixed, along with 10 mL of a 4.8% PVA solution. The mixture was continuously stirred at room temperature for 2 h. A mixture of 0.03 mmol of DHEBA (0.006 g), 0.697 mol of MAA (0.060 g), 0.02 g SLS, 12.0 mL of distilled water, and 10 mL of 4.8% PVA was added into the mixture to ensure dispersion of the powder in the toluene. The mixture was kept stirring overnight at  $50^\circ\text{C}$  under a stream of nitrogen. The supernatant liquid was homogenized at 1,000 bars for 1 h, and the resulting particles (less than 100 nm) were obtained. The extraction of template would affect to a low and variable absorption of the binding template, so we performed the removal of the template from the obtained polymer by a skin dialysis using Snake skin<sup>®</sup> Dialysis Tubing (Thermo Fisher Scientific Inc., USA) against methanol (100 mL) for three times. The complete removal of the template from the polymer matrix was verified by the analysis of rinses by chiral HPLC analysis. A non-imprinted polymer (NIP) was used as the control which was prepared in the same way as the MIP beads except the addition of template.

**Table 1: The composition of the polymer of molecularly imprinted polymers.**

Polymer	Template (mol)	PS (g)	MAA (mol)	NVP (mol)	DHEBA (mol)	AIBN (mmol)
MIP1	0.025	1.0	0.43	0.17	0.03	0.73
MIP2	0.025	1.0	0.35	0.35	0.03	0.73
MIP3	0.025	-	0.43	0.17	0.03	0.73
MIP4	0.025	-	0.35	0.35	0.03	0.73

## 2.3. Characterizations of MIP

It is important to verify the MIP after the polymerization process and the real performance of all the MIPs, which the obtained MIP and NIPs were characterized using an non-contact mode AFM, SPA400 AFM (SEIKO Inc., Chiba, Japan). This technique is advantageous to image and manipulate atoms and structures on a variety of surfaces for a  $5 \mu\text{m} \times 5 \mu\text{m}$  area of the sample that was scanned to probe the surface patterning in air at room temperature ( $25 \pm 1^\circ\text{C}$ ) and at a scan speed of 1 Hz. The AFM tip consisted of a pyramidal  $\text{Si}_3\text{N}_4$  (typical radii: 10 nm for etched Si tip). A silicon cantilever was used with a typical spring constant of 20 N/m in the tapping mode and a scan speed of 1 Hz. The precisely surface analysis method can be used to analyze topography using software Nano Navi SPA400 (DFM). Upon image analysis, the nanosized topography of MIPs was measured with the distinct forces in dynamic force microscope mode by scanning a  $1 \mu\text{m} \times 1 \mu\text{m}$  area using a HA-NC cantilever, Etalon probe with 110-190 kHz resonance frequencies. A constant force was used in the range of  $2.5\text{-}10 \text{ N m}^{-1}$ . All the experiments were performed at room temperature ( $25 \pm 1^\circ\text{C}$ ).

## 2.4. Sensor measurement

The adsorption affinity achieved by the MIP-based sensor, was performed when thalidomide enantiomer was exposed to MIPs on the sensor. The measured data from all the MIPs and NIPs were plotted as a function of the thalidomide enantiomer concentrations range from 0.01 to 100  $\mu\text{g/mL}$ . Correlation coefficients were evaluated for each enantiomer with and without the incubated lipid serum in the blood. Standard solutions of the enantiomer concentrations were prepared from each diluted aliquots. After washing the template of MIP sensor, the reproducibility of the signal changes between the bare electrode and MIPs and the analysis protocol corresponded to the ICH guideline (ICH, 2005). The standard deviation was less than 10% relative to background signals, this is to ensure extraction of unreacted species and the bound template before analysis of template, hence the sensitivity of detection. The selectivity and imprinting coefficients were calculated to determine the efficiency of the imprinting approach. All experiments were carried out in triplicate at room temperature ( $27 \pm 1^\circ\text{C}$ ). For the effective diffusion coefficients ( $D_B$ ), calculation of the resistance data was done either with or without the lipid-protein, in terms of water loss and capacitance due to the altered vapor pressure (Nilsson 1977) in Eq. 1:

$$D_B = \frac{D_o M(T)^{1.75} \times 101 \times 10^3}{RTCP_{sat}} \quad \text{Eq. 1}$$

, where  $D_o$  is diffusion coefficient of the water-vapor-air mixture ( $2.5 \times 10^{-5}$ ),  $M$  is molecular weight of thalidomide ( $M = 258 \text{ g/kmol}$ ),  $P$  is the saturated vapor pressure ( $7.21 \text{ mmHg}$ ),  $C$  is capacitive resistance,  $R$  is the gas constant ( $6.314 \text{ JK}^{-1} \text{ mol}^{-1}$ ) and  $T$  is temperature in kelvin.

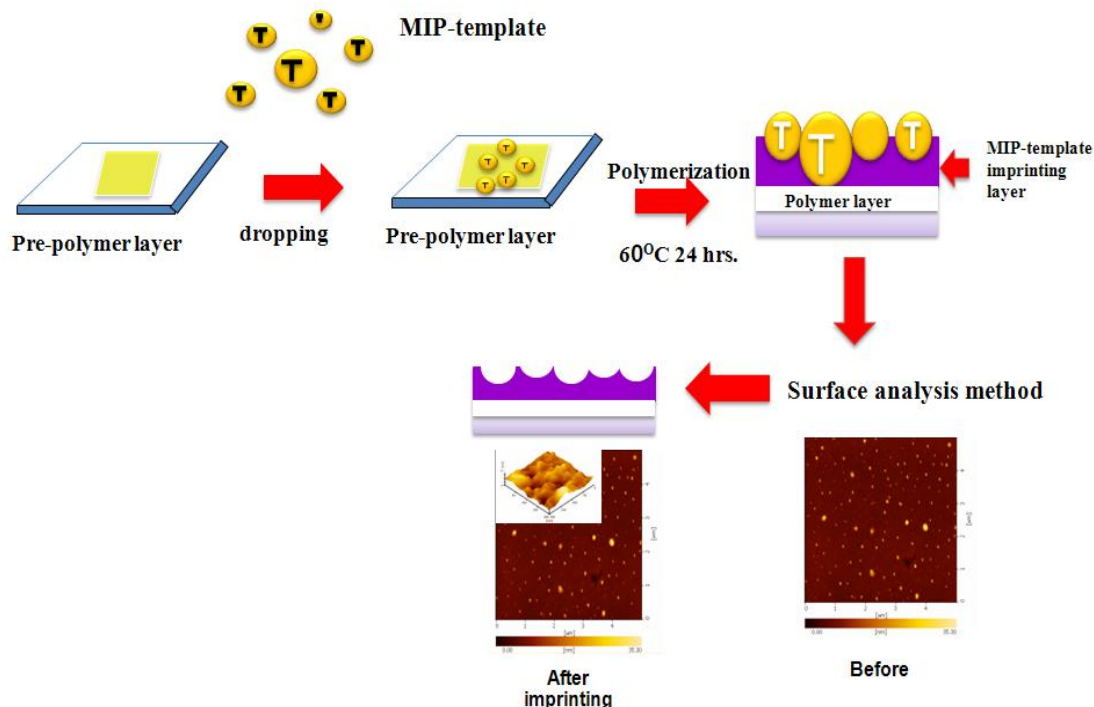
### 2.5. AFM with confocal Raman microscopy (AFM-Raman)

The functional organization of the molecularly imprinted polymer were evaluated that the advantage of technology of visualization is transformation of images and the input of the sample using AFM combined with Raman. The Raman system (NT-MDT, Moscow, Russia) consisted of a 35-mW He-Ne excitation source of 632.8 nm and a power of 10-12 mW with a spot size of 1  $\mu\text{m}$ . The Stokes-shifted Raman scattering was recorded using a 1200 grove  $\text{min}^{-1}$  grating and a Peltier-cooled charged-coupled device for sample coating materials ( $1 \times 1 \mu\text{m}$ ), the silver substrate by the RF magnetron sputtering with a thickness of 200 nm, RF power of 150 W, and an Ar flow rate of 20 scan. Identification of individual surface atom, chemical interactions changed the tip vibration frequencies to be detected and mapped, capable of distinguishing atoms in the presence of interference contribution. The SERS enhancement (1-10  $\text{\AA}$  resolution) renders a high resolution with less interference exposed to the MIPs (CCD; Andor Technology PLC, California, USA) with the neglected noise of the background (Wang and Irudayaraj, 2013). To determine each point in the AFM, Raman spectroscopy was used to confirm structure of the compounds. Multiple spectra were acquired with exposure times of 10 s using an accumulated time 12 N. In addition, the specification for Raman-AFM was kept the same throughout the process under ambient conditions.

## 3. Results and discussion

### 3.1. Synthesis of the MIPs

**Scheme 1:** Schematic illustration of the preparation of the configurational biomimesis (R)- and (S)-thalidomide-molecularly imprinted polymer as a platform for the evaluation of drug delivery in this study.



Scheme 1 provides a schematic representation of the configurationally biomimesis molecularly imprinted polymers obtained in this study. The copolymer of the methacrylate-bound imprint cavities consisted of the H-bonding interaction and the anionic carboxyl ate group of the monomer. The DHEBA was used as a cross linker, which consisted of two hydroxyl groups. The additional advantage of the present MIP as that was expected to maintain the stability of the molecular structure for fine-tuning of the specific target area after the template

removal (Petcu et al., 2009). Further the non-contact mode AFM image of MIPs (core-shell) and the corresponding NIP revealed that the cavitated particles near the non-imprinted polymer region and some toughness of the particles remained on the polymer coating, while the roughness was measured from the magnitude on image analysis.

**Table 2: AFM image analysis for both the MIPs and corresponding NIP.**

Parameters	NIP	RMIP	SMIP
Particles dimension (mean, n=3) nm	78.41	53.15	48.35
Film thickness (z scale)	12.46	10.98	2.32
Distance of a pair of particle ( $\Delta Z$ scale = Z1-Z; nm)	1.36	0.53	0.18
Roughness (amplitude, nm)	0.76	0.48	0.27

Table 2 shows the image analysis of the MIPs and corresponding NIP obtained by the cavitation method. As can be seen, the internal structure of a pair of particles, corresponding with different distances in pair of the pattern of adjacent nanoparticles for RMIP is 2-fold higher than that in SMIP. Moreover, the toughness increased toward the increasing of content rendered the reaction was carried out at room temperature resulted in a well-defined shape for both the template molecules, after the removal of the template. The result clearly indicated that each of the template enantiomer affected to the imprinted cavities differently. The AFM image of NIPs revealed that they do not transition well in all the cases, in part, also accounted for the nature of the cavities that were formed. In addition, NIP showed a high value for height against the thickness (as measured by Z scale), was comparable to RMIP is 5-fold higher than that for SMIP which was the thinnest. When the roughness is compared in both MIPs, also NIP this has the same trend as the thickness. This could be explained by different contact geometry due to of the MIPs prepared using the present imprinting techniques (Hooton et al., 2004).

### 3.2. Characteristics of the MIPs

A surface analysis method that offers the determining the structure was initially used as template, remained prior to use by using AFM images. In initial study, (*R*)- and (*S*)-thalidomide imprinted polymers have been prepared based on the surface imprinting techniques. Varying of the surface properties can be used to adjust the functionalities on the imprinted cavity using AFM images. Two sets of MIPs were thus prepared – one with poly(styrene); MIP1 and MIP2 and the other without poly(styrene); MIP3 and MIP4 – in an oligomer film onto a glass substrate. MIP1 and MIP3 composed of 0.35 mole ratio of MAA, or NVP functional monomer only, MIP2 and MIP4 noncore-shell prepared in MAA:NVP at 0.43:0.17 were studied (the polymer composition as shown in Table 1). All of the MIPs had the nano sizes (less than 100 nm) after homogenization and the dialysis (Thermo Fisher Scientific Inc., USA) as determined by a zeta nanosizer technique. We performed compositional analysis of MIPs in comparison to the corresponding NIPs by dynamic image analysis if the monomers are incorporated at the ratios given in the pre-polymer prior to enantiomer analysis. A study of the interactive forces with the AFM applying the force to the cantilever, when the tip touched and pressed the sample, showed that it was able to probe the small interaction area (constant force of  $\text{Nm}^{-1}$ ). The present technique provided high sensitivity to a small force on the AFM images for all the MIPs in this study. The force values of (*R*)-thalidomide for RMIP1 were the highest at 1,400 nN compared with the other MIPs. In addition, the AFM images of MIPs showed hysteresis in all of the RMIPs, except that for RMIP1. Such forces of the former materials were lower than those of RMIP4 (1,100 nN). In contrast, the (*S*)-thalidomide imprinted polymer had a relatively smaller force with a value of about 55-80 nN for all cases of SMIPs (Figure 1e).

The force values of all NIPs, either for (*R*)-thalidomide or (*S*)-thalidomide, were less than 100 nN, which were similar and not relevant to the polymerized monomers of the polymer composition. A large increase in the force values on RMIP1 and the absence of hysteresis appeared during the retraction of the force-distance curve (see Figure 1f) compared to the other RMIPs and SMIPs (see Figures 1e and f), also NIPs for both the enantiomers

(Figures 1g and h), owing to the changes in surface adhesion of functionalities, barrier friction, or orientation of molecules.

**Figure 1:** (a) The force values of (R)-thalidomide and (b) (S)-thalidomide MIPs from AFM images, (c) the roughness values, and (d) separation distances of the various MIPs and NIPs. The force curves of the different MIPs; (e) SMIP, (f) RMIP, (g) NIP-S, (h) NIP-R.

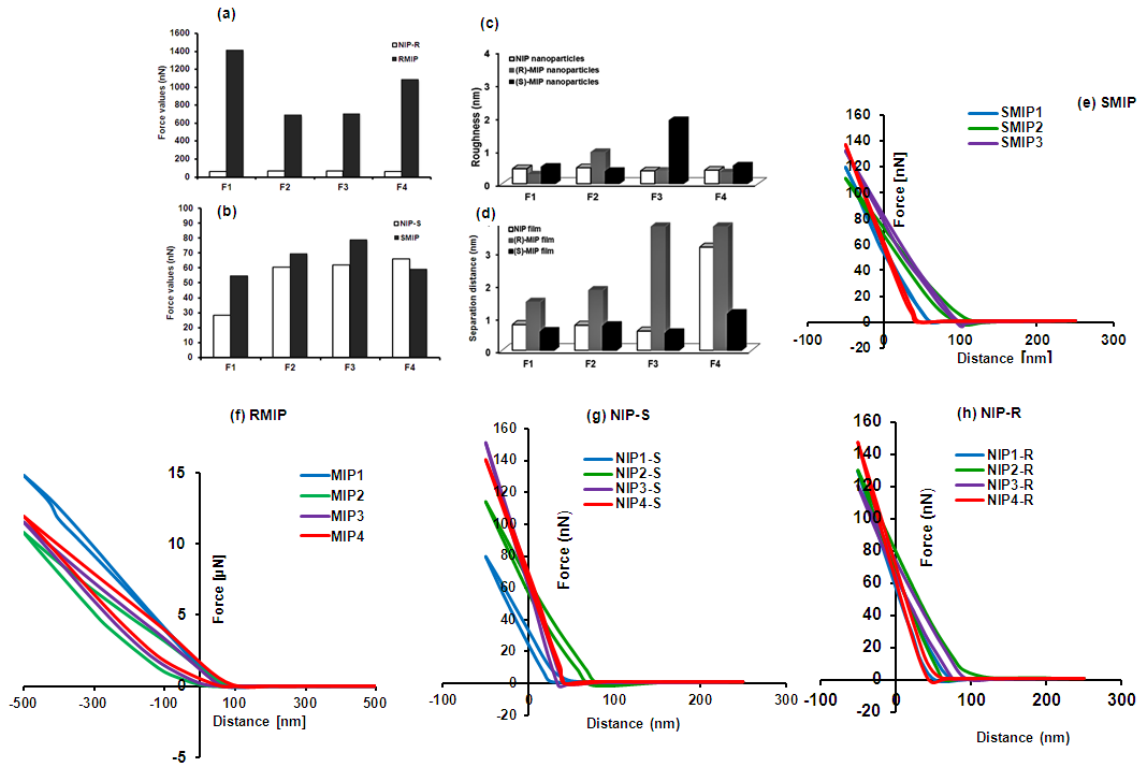
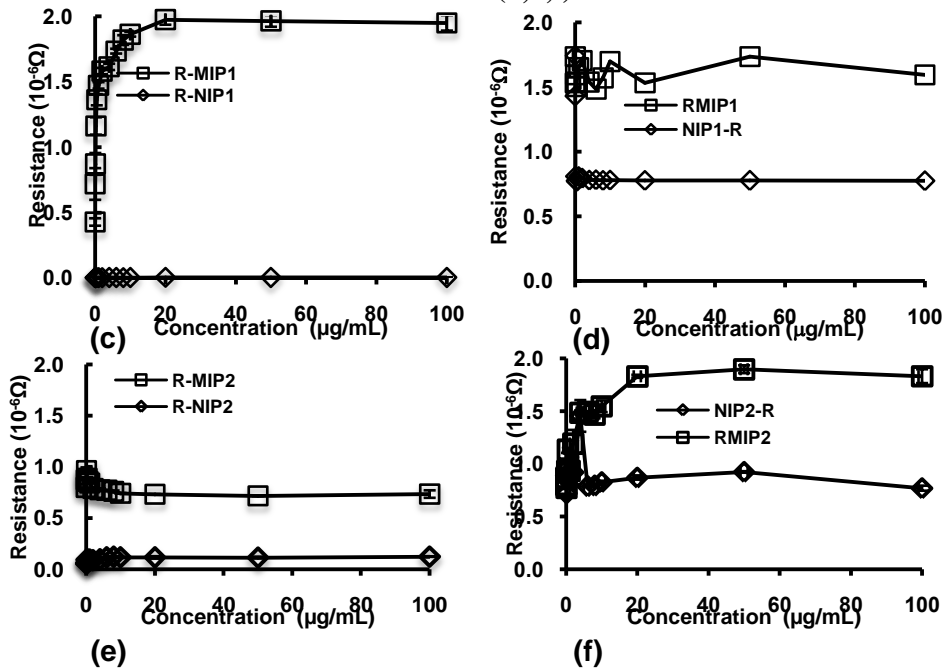


**Figure 2:** The sensor measurement of the (R)-thalidomide on RMIPs and NIPs without (a,c,e) and with the blood (b,d,f).



**3.3. The sensor measurement of thalidomide with the blood**

Next, the study of thalidomide release based on the MIP-sensor was performed that is suitable technique as it is capable of continuous monitoring of the blood. To select the optimal material for application, sensor measurement between 0.01 and 100  $\mu\text{g/mL}$  was recorded in the presence of bovine serum albumin and lipid compounds for all the MIPs (Figure 2a,b). Because the interaction of platelet to endothelial cells adhesion and leukocytes in early stage that change the signal measurement against the protein matrix onto the nano material. In the typical sensor measurements, impedance values of the MIP gradually increased upon sequentially dropped analytes, while the addition of the blood, this turns up, which can show fluctuated signal for RMIP1. Obviously, the observation of differences between both the enantiomers was consistency for the RMIPs, at a lower concentration (0.01-1  $\mu\text{g/mL}$ ), and increased between 1 and 20  $\mu\text{g/mL}$ , beyond that the trend leveled off. The values of RMIP2 and RMIP4 gradually increased in the range of 1-20  $\mu\text{g/mL}$  of (*R*)-thalidomide after the added blood shifted the response at higher magnitudes in Figure 2(d,f). In contrast to all the cases of NIPs, a signal can be discriminated from the baseline while the sequentially addition of (*R*)-thalidomide with the blood up to 100  $\mu\text{g/mL}$ . Upon sensor measurement, the protein matrix did not affect to the level for the SMIPs in the range of 0.01-100  $\mu\text{g/mL}$  of (*S*)-thalidomide. Also, the SMIPs could measure different signals between without and with the blood, except SMIP4 that the level dropped to a lower level before reaching to a stable baseline beyond 20  $\mu\text{g/mL}$ . Overall, the  $D_B$  of RMIPs is shown approximately  $1 \times 10^5 \text{ m}^2/\text{s}$  to  $5 \times 10^5 \text{ m}^2/\text{s}$  in all the cases. An excellent sensor response, which indicated  $D_B$  value was calculated and was found to be about  $480 \times 10^5 \text{ m}^2/\text{s}$  for SMIP3, while that of  $6 \times 10^5 \text{ m}^2/\text{s}$  for SMIP4 in the blood was exposed to the surface of electrode, showing long-range with the *S*-enantiomer template. There was a far better difference in performances distinguishing the blood component on all of the core-shell RMIPs and SMIPs, but was not for non-core-shell MIPs, especially in SMIP4 because it was not comparable to the sample solution alone.

### 3.4. The analytical data of the thalidomide sensor

In the impedance measurement of the optimal MIP1, we focused on the analysis of the (*R*)-thalidomide enantiomer in a phosphate buffer (pH 5.5) and acetonitrile (1:1, mixture) for a non-racemic mixture, which linearity ( $R^2$ ) > 0.985 was achieved, as shown in Figure 5a,b. The plot from the MIP1 sensor revealed that the slope value unity for (*S*)-enantiomer but is not the case for (*R*)-enantiomer on the MIP-based sensor. As shown in Table 4, the sensitivity of the SMIP1 was not changed between with and without the protein matrix and the RSD values were lower than 0.86%. Meanwhile, the sensitivity of the RMIP1 sensor for (*R*)-thalidomide was different with and without the blood, a factor of 2-fold, wherein the substantial high RSD value (9.04%) was found for the (*R*)-thalidomide with blood.

**Table 3: The analytical data and linearity of the thalidomide enantiomers for MIP1 using impedance measurement.**

Substance	Thalidomide enantiomer	Slope	Linearity ( $R^2$ )	LOD* (ng mL <sup>-1</sup> )	LOQ** (ng mL <sup>-1</sup> )	%RSD
without matrix	<i>R</i> -	0.119	0.987	0.76	1.15	9.04
	<i>S</i> -	0.172	0.985	0.62	1.00	0.86
with matrix	<i>R</i> -	0.057	0.990	6.40	21.27	0.80
	<i>S</i> -	0.172	0.996	0.53	0.63	0.63

\* LOD is the lower limit of detection

\*\*LOQ is the lower limit of quantification

**Table 4: The selectivity of MIP (NIP/MIP ratio) and the thalidomide enantiomers ( $\text{\AA}$ ) penetrated into the blood component by the localized Raman-AFM.**

Polymer	Without		With the blood mixture			
	<i>R</i> -form	<i>S</i> -form	<i>R</i> -form		<i>S</i> -form	
	NIP/MIP*	NIP/MIP*	( $\text{\AA}$ )	NIP/MIP*	( $\text{\AA}$ )	NIP/MIP*
MIP1	731.9 $\pm$ 86.2	18,051 $\pm$ 685	1.22 $\pm$ 0.29	2.03 $\pm$ 0.06	0.74 $\pm$ 0.17	1.06 $\pm$ 0.05
MIP2	6.74 $\pm$ 0.20	1.59 $\pm$ 0.05	1.04 $\pm$ 0.21	2.11 $\pm$ 0.08	1.88 $\pm$ 0.20	44.45 $\pm$ 2.34
MIP3	308.4 $\pm$ 22.4	1,248.12 $\pm$ 289	1.65 $\pm$ 0.16	0.37 $\pm$ 0.01	1.65 $\pm$ 0.21	0.01 $\pm$ 0.00
MIP4	2.12 $\pm$ 0.06	786.67 $\pm$ 75	1.75 $\pm$ 0.21	0.43 $\pm$ 0.01	1.78 $\pm$ 0.14	12.24 $\pm$ 4.28

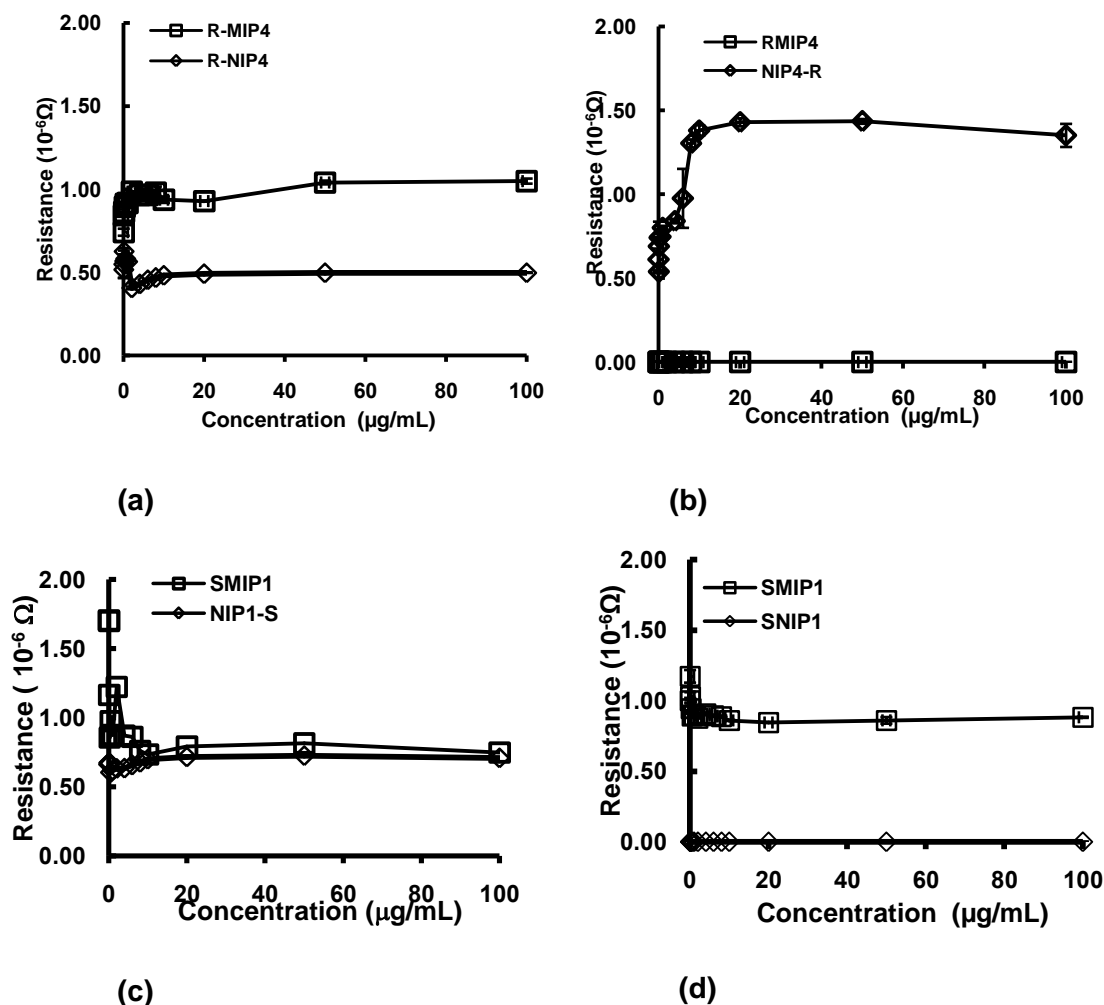
\*P value < 0.001 in comparison between MIPs and NIPs, for all the cases.

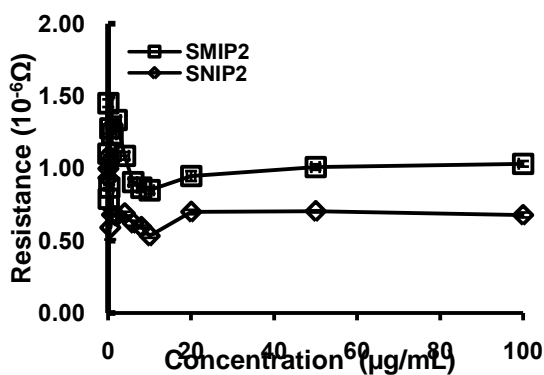
### 3.5. The selectivity of the thalidomide enantiomers from the MIPs

The selectivity of MIPs (NIP/MIP ratio) that examine effective diffusion coefficient [ $D_{e(ss)}$ ] by diffusion coefficient ( $D_m$ ) for thalidomide enantiomers with and without the blood. The imprinting factor, which is the ratio of the binding affinity of the template from the MIP of supported the polymer, was examined for four MIPs (see Table 4). In comparing the MIP2, high selectivity was observed for both the enantiomers with the blood, same as the MIP4. The imprinted polymer exhibited an increased affinity to template with respect to NIPs and showed pronounced selectivity of the NIP/MIP ratio were comparable among the two enantiomers prior to the adding of the blood component (Table 4). And, the imprinted polymers, SMIP1 and SMIP2 showed that a high amount of thalidomide was adsorbed and released into the solution, while SMIP3 and SMIP4 show higher interactions in the adsorption toward the template against the protein matrix where was adsorbed inside the MIP. This data was compared with effective diffusion coefficient of NIP, clear corresponded to the AFM images of NIPs. SMIPs compared to those for all the case of RMIPs which showed the selectivity (NIP/MIP) or (MIP/NIP) approximately of 2-fold for the MIP. Meanwhile, upon the exposure to the blood, the SMIP2 showed the imprinting efficiency about 45-fold. On the other hand, selectivity (NIP/MIP) was achieved for 12-fold of the SMIP4 (see Table 4). After the addition of the blood component, there was substantial difference of impedance signal which this can be attributed to the template exposed to MIPs prepared using a higher mole ratio of MAA than NVP. The results indicated that this technique based on MIP could distinguish the required time for different diffusive paths among the other form and the desired enantiomer on the various coating barriers established.

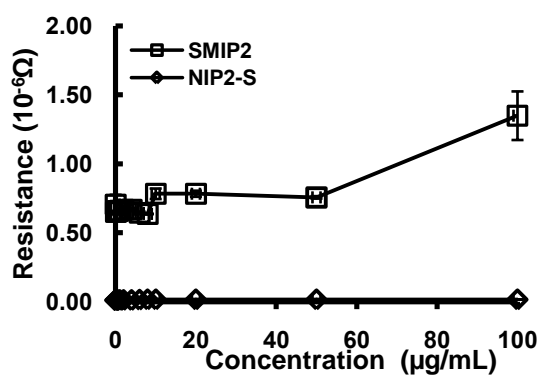
### 3.6. The imaging and force measurement

**Figure 3: The sensor measurement of the (S)-thalidomide on SMIPs and NIPs without (a,c,e) and upon exposure to the serum lipids in the blood (b,d,f).**

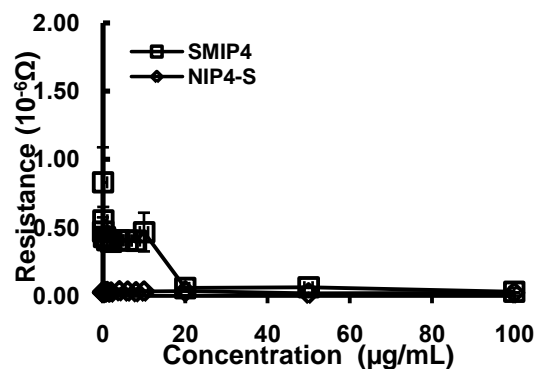
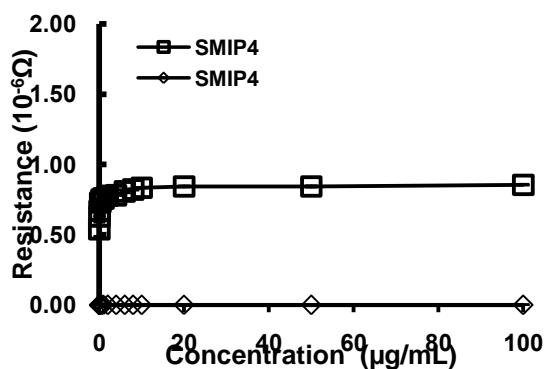




(e)



(f)



To test the influence of the whole blood on the detection of target, we needed to improve its sensitivity by atomic force microscopy technique. AFM is advantageous to image and study in trival details of the localized binding site on the variety of surfaces (Hooton 2004). We anticipated that this technique would provide the strong support of the parameter from the sensor measurement with increased consistency, and enhanced scrutiny should be addressed to assessing of a drug remained in the protein matrix. The AFM, MIP with surface-enhanced analysis using a silver tip provided object classification (Feng 2015). Totally different images from AFM of MIP1 that manipulated the 2D array from the blood component was shown in Figure 5(c and d).

In addition, the correlation to the shift with the surface impression on the Raman-AFM is not a mere pore, and is used to detect the template molecules in-depth successfully on the images. As illustrate in Table 4, the identification 10 different objects on each AFM image of the MIPs exposure to the blood with respective confident intervals (11%-20%). Furthermore, the AFM combined with Raman on the images (approximately of  $x = 10$  nm, as determined by the  $z$  scale of AFM images). Furthermore, the results for the RMIP2 showed correlating to the force curve (see Figure 6); the force of (*R*)-thalidomide (130 nN) was about three-fold higher than that for (*S*)-thalidomide (40 nN). The images from contact mode AFM showed a large coalescence of the interferences, in Figure 6a (left), while the cloud dense exposed to a core-shell SMIP2, in Figure 6b (left), respectively.

**Figure 5:** The sensitivity of the sensor measurement for MIP1; (a) (*R*)-thalidomide and (b) (*S*)-thalidomide that was exposed to thalidomide sensor for MIP1. (c) AFM image upon exposure to the blood, differently between; (*R*)-thalidomide-MIP and (d) (*S*)-thalidomide-MIP on sensor.

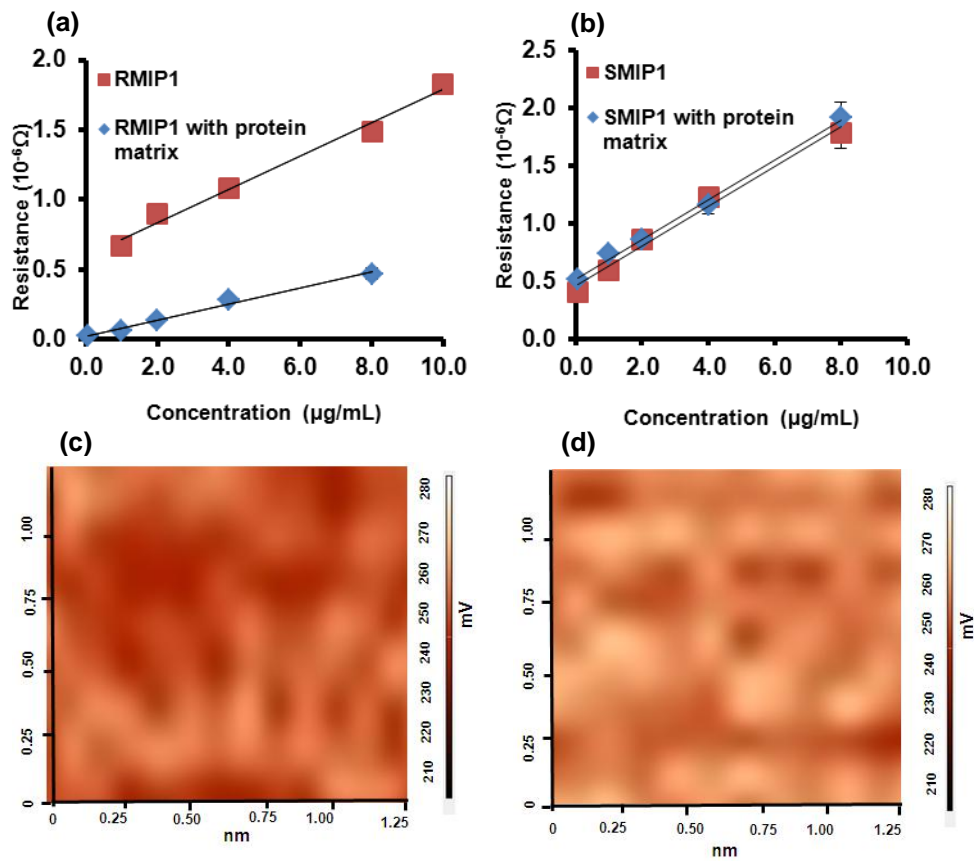


**Figure 6:** Comparison of force curves of the MIP2 on IDCin Raman-AFM images upon exposure to the proteolipid in the blood; (a) (*R*)-thalidomide and (b) (*S*)-thalidomide. The nanoscale contact geometry on the glass substrate for  $1 \times 1 \mu\text{m}$  and  $z = 40$  and  $100 \text{ nm}$ .

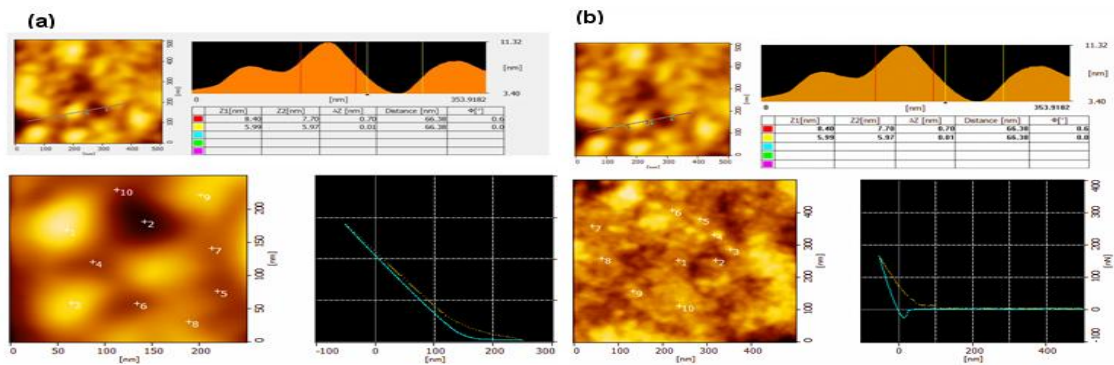
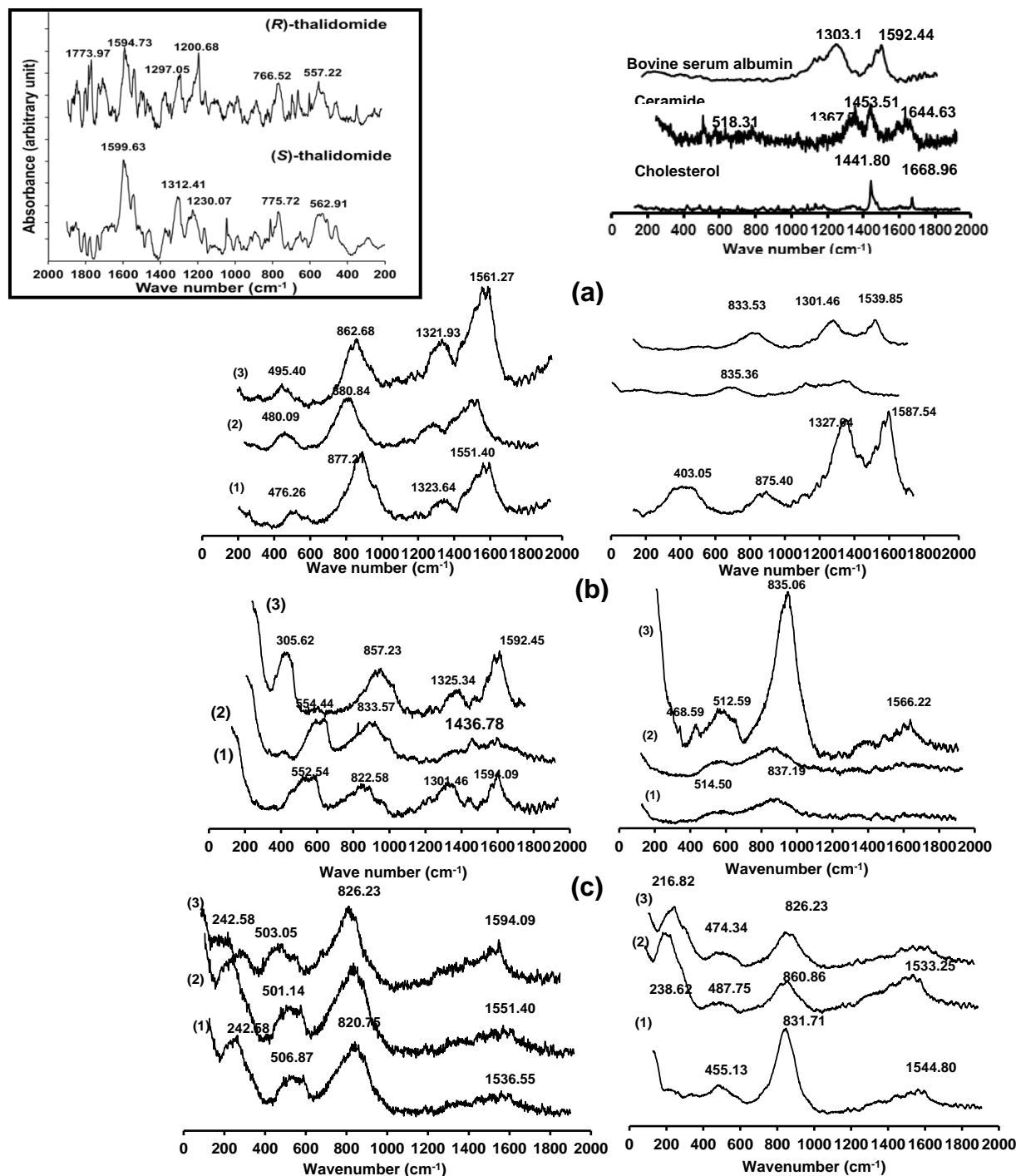


**Figure 7:** The Raman spectra from various regions on the sensor. **Left:** the (a) RMIP-1, (b) RMIP-2, and (c) RMIP-4; **Right:** (a) SMIP-1, (b) SMIP-2, and (c) SMIP-4, (insert, right) Raman for each of blood component, and (insert, left) (*R*)-, and (*S*)-thalidomide is given for comparison.



The differences between AFM and Raman, and force on the images should correspond to an increase in volume of the template enantiomer within the protein matrix exposed on nano-imprint, as shown in Table 4. The chemical functionalities of the imprinted site were responsible for the promotion of rebinding ability and high selectivity. So, the obtained MIPs, especially in the core-shell type were capable of distinguishing thalidomide in spite of interference in the whole blood. Taking together the results from force measurement and the images and Raman on the AFM demonstrate, MIP1 and MIP2 can be used to distinguish different nanomaterials in the whole blood and to visualize the interferences, compared to the corresponding NIP control polymers.

The optimal surface property of MIP1 led to assessing the differences from sensor measurement with and without the blood. The results clearly indicated that the core-shell, with the property of poly(styrene) is an important that can generate selectively arrangement of templating species by surface imprinting technique. Next, in Fig. 7, Raman, which focus precisely for the intrinsic structure of the template on respective MIP2 on the AFM images, to compare with forces that thalidomide accommodated readily in regional difference for this MIP. Compare among the MIPs, Raman of RMIP2 showed the differential peaks that amide band of the blood cell component appeared, at  $1300\text{ cm}^{-1}$  and  $1500\text{ cm}^{-1}$ , and overlapped with the abundant peak at  $1441\text{ cm}^{-1}$  (see Figure 7a). However, (*R*)-thalidomide at  $1436\text{ cm}^{-1}$  highlighted functionalities of this MIP2 exposed to the blood, indications at  $1300\text{ cm}^{-1}$  and  $1500\text{ cm}^{-1}$  (Wang, Irudayaraj 2013). The Raman shift showed (*S*)-thalidomide was distinctly a peak at about  $835\text{ cm}^{-1}$  in sensor response, in Figure 7b, due to isotopic pattern and the Raman shift. This work highlighted an enhanced ability of MIP, especially in core-shell, assembled rotation and transformation in the treated sites, hence correlated the signals measured secondarily apart which we observed from the increased intensity of signal-to-noise ratio (Barahona et al., 2013).

#### 4. Conclusion

In this study, we demonstrate that the configurationally biomimesis imprinting approach created more efficient drug-MIP interaction. The release of the template led to change of impedance which involved the behavior of the perturbation of the lipids, essential constituents of protein matrix in the blood. It seems, however, that the type of MIP with core-shell overcomes for this with property which contributed the contamination of interferences can be diminished is as a direct measurement of delivered target. Considering to the results of clear performance in a response of known therapeutic through changes within the blood, the strategy of varying in the chemical functionalities resulted in favorable nanomaterial, depending on minor change of templates. The serum protein-lipids derived from cell death activate, that possessed a blood abnormality, or even complex (e.g. kidney damage, stroke and inflammatory). The attempt of our investigations aimed to reducing the risk increased in the death or complicated treatment in the patients. The work indicated that present MIPs provide potential as recognition material for drug assessment shed the light on drug delivery to the vascular system and factoring on problem in an early stage.

#### Acknowledgements

Financial support is gratefully acknowledged from the Higher Education Research Promotion and National Research University Project of Thailand for Ph.D. scholarship (Code no. PHA 540545d), Office of the Higher Education Commission and the Drug Delivery System Excellence Center at Prince of Songkla University and the Nanotechnology Center (NANOTEC), NSTDA, Ministry of Science and Technology, Thailand, through its program of Center of Excellence Network. We thank you to Miss Wanpen Naklua for blood sample, Dr. Sreenu Madhumansi for the correction in the English and this work is dedicated to Dr. Brian Hodgson in memory.

#### Declaration of Interest

The authors report no declaration of interest. The authors are solely responsible for the content of the paper.

#### References

- Arabi, M., Ghaedi, M. & Ostovan, A. (2017). Development of a lower toxic approach based on green synthesis of water compatible molecularly imprinted nanoparticles for the extraction of hydrochlorothiazide from human urine. *ACS Sustainable Chemistry & Engineering*, 5, 3775-3785.
- Barahona, F., Bardliving, C. L., Phifer, A., Bruno, J. G. & Batt, C. A. (2013). An apt sensor based on polymer-gold nanoparticle composite microspheres for the detection of marathons using surface-enhanced Raman spectroscopy. *Industrial Biotechnology*, 9, 42-50.
- Beedie, S. L., Mahony, C., Walker, H. M., Chau, C. H., Figg, W. D. & Vargesson, N. (2016). Shared mechanism of teratogenicity of anti-angiogenic drugs identified in the chicken embryo model. *Scientific Reports*, 6, 30038 (1-10).
- Bellagha-Chenchah, W., Sella, C., Fernandez, F. R., Peroni, E., Lolli, F., Amatore, C., Thouin, L. & Papini, A. M. (2015). Interactions between human antibodies and synthetic conformational peptide epitopes: Innovative approach for electrochemical detection of biomarkers of multiple sclerosis at platinum electrodes. *Electrochemical Acta*, 176, 1239-1247.

- Byrne, M. E., Hilt, J. Z. & Peppas, N. A. (2008). Recognitive biomimetic networks with moiety imprinting for intelligent drug delivery. *Journal of Biomedical Materials Research Part A*, 84A, 137-147.
- Chen, Y. W., Rick, J. & Chou, T. C. (2009). A systematic approach to forming micro-contact imprints of creatine kinase. *Organic & Biomolecular Chemistry*, 7, 488-494.
- Eersels, K., Lieberzeit, P. & Wagner, P. (2016). A review on synthetic receptors for bioparticle detection created by surface-imprinting techniques—from principles to applications. *ACS Sensors*, 1, 1171-1187.
- Feng, S. & Lu, X. (2015). Molecularly imprinted polymers integrated with surface enhanced Raman spectroscopy: Innovative chemosensory in food science. *Lipid Technology*, 27, 14-17.
- Haginaka, J., Takehira, H., Hosoya, K. & Tanaka, N. (1998). Molecularly imprinted uniform-sized polymer-based stationary phase for naproxen: Comparison of molecular recognition ability of the molecularly imprinted polymers prepared by thermal and redox polymerization techniques. *Journal of Chromatography A*, 816, 113-121.
- Hattori, Y., & Iguchi, T. (2004). Thalidomide for the treatment of multiple myeloma, 44, 125-136.
- Hooton, J. C., German, C. S., Allen, S., Davies, M. C., Roberts, C. J., Tendler, S. J. B. & Williams, P. M. (2004). An atomic force microscopy study of the effect of nanoscale contact geometry and surface chemistry on the adhesion of pharmaceutical particles. *Pharmaceutical Research*, 21, 953-961.
- International Conference on Harmonization of Technical Requirements for Registration of Pharmaceuticals for Human Use, ICH Harmonized tripartite guideline. Validation of analytical procedures: text and methodology Q2(R1), Current step 5 version, Geneva, 2005.
- Karlsson, B. C. G., O'Mahony, J., Karlsson, J. G., Bengtsson, H., Eriksson, L. A. & Nicholls, I. A. (2009). Structure and dynamics of monomer-template complexation: An explanation for molecularly imprinted polymer recognition site heterogeneity. *Journal of the American Chemical Society*, 131, 13297-13304.
- Kryscio, D. R., & Peppas, N. A. (2012). Critical review and perspective of macro molecularly imprinted polymers. *Acta Biomaterialia*, 8, 461-473.
- Liang, J., Wu, Y. & Deng, J. (2016). Construction of molecularly imprinted polymer microspheres by using helical substituted polyacetylene and application in enantio-differentiating release and adsorption. *ACS Applied Materials & Interfaces*, 8, 12494-12503.
- Nilsson, G. E. (1977). Measurement of water exchange through skin. *Medical and Biological Engineering and Computing*, 15, 209-218.
- Owens, P. K., Karlsson, L., Lutz, E. S. M. & Andersson, L. I. (1999). Molecular imprinting for bio- and pharmaceutical analysis. *Trends in Analytical Chemistry*, 18, 146-154.
- Petcu, M., Karlsson, J. G., Whitcombe, M. J. & Nicholls, I. A. (2009). Probing the limits of molecular imprinting: strategies with a template of limited size and functionality. *Journal of Molecular Recognition*, 22, 18-25.
- Sellergren, B. (1994). Direct drug determination by selective sample enrichment on an imprinted polymer. *Analytical Chemistry*, 66, 1578-1582.
- Suedee, R., Intakong, W. & Dickert, F. L. (2006). Molecularly imprinted polymer-modified electrode for on-line conductometric monitoring of haloacetic acids in chlorinated water. *Analytica Chimica Acta*, 569, 66-75.
- Tabane, T. H., & Batlokwa, B. S. (2017). A novel molecularly imprinted polymer for the selective removal of interfering hemoglobin prior to whole blood analysis. *Biochemistry & Analytical Biochemistry*, 6, 1000315 (1-7).
- Vyacheslav, A. K., Stephen M. S., & Bradford C. B. (2007). Vascular remodeling: Hemodynamic and biochemical mechanisms underlying Glagov's phenomenon. *Journal of the American Association*, 27, 1722-1728.
- Wang, Y. & Irudayaraj, J. (2013). Surface-enhanced Raman spectroscopy at single-molecule scale and its implications in biology. *Philosophical Transactions of the Royal Society B: Biological Sciences*, 368, 20120026 (1-10).
- Xing, R., Wang, S., Bie, Z., He, H. & Liu, Z. (2017). Preparation of molecularly imprinted polymers specific to glycoprotein's glycan and monosaccharide's via boronate affinity controllable-oriented surface imprinting. *Nature Protocols*, 12, 964-987.
- Yabu, T., Tomimoto, H., Taguchi, Y., Yamaoka, S., Igarashi, Y. & Okazaki, T. (2005). Thalidomide-induced antiangiogenic action is mediated by ceramide through depletion of VEGF receptors, and is antagonized by sphingosine-1-phosphate. *Blood*, 106, 125-134.